American Mineralogist, Volume 102, pages 1718–1726, 2017

Analysis of erionites from volcaniclastic sedimentary rocks and possible implications for toxicological research

MARTIN HARPER[1,*], ALAN DOZIER[2], JULIE CHOUINARD[3], AND ROBYN RAY[4]

[1]Exposure Assessment Branch, Health Effects Laboratory Division, National Institute for Occupational Safety and Health, 1095 Willowdale Road, MS-3030, Morgantown, West Virginia 26505, U.S.A.
[2]Chemical Exposure & Monitoring Branch, Division of Applied Research & Technology, National Institute for Occupational Safety & Health, 1090 Tusculum Avenue, MS-R7, Cincinnati, Ohio 45226, U.S.A.
[3]Center for Advanced Materials Characterization in Oregon (CAMCOR), University of Oregon, 1443 E. 13th Avenue, Eugene, Oregon 97403, U.S.A.
[4]EMSL Analytical, Inc., 200 Route 130 North, Cinnaminson, New Jersey 08077, U.S.A.

ABSTRACT

Erionite occurs in volcaniclastic rocks and soils; in some villages in Turkey the presence of erionite in local rocks is associated with mesothelioma, a disease also associated with inhalation of airborne asbestos. Since volcaniclastic rocks containing erionite are widely present in the western U.S.A., there is a concern over potential health issues following inhalation of dust particles in these areas and thus there is a need to identify and quantify erionite particles found in air samples during hygienic investigations. Previous attempts to analyze the few micrometer-sized erionite particles found on air sample filters under transmission electron microscope (TEM) encountered difficulties due to electron beam damage. Recommendations are presented for accurate analysis by both energy-dispersive spectroscopy (EDS) and selected-area electron diffraction (SAED). Much of the work previously published to establish the crystal chemistry of erionite has involved the relatively large crystals found in vesicles in extrusive volcanic rocks. Analysis of these crystals gives a weight percent ratio of Si to Al in a narrow range around 2.7 (molar ratio 2.6), consistent with a unit-cell formula $Al_{10}Si_{26}$. In addition, the cation contents of these crystals generally meet the charge balance error formula for zeolites. However, erionites formed in volcaniclastic sedimentary rocks (tuffs) have very different Si:Al weight percent ratios, around 4.0, which is above the upper range for the analyses of the crystals found in vesicles. Analysis of many particles in samples from different locations reveal two other major differences between the erionites from the sedimentary situations and those found in vesicles. (1) The extra-framework alkali cation (Na, K, Ca) contents are lower than required for a stoichiometric balance with framework Al substitution for Si so that the cation charge balance error formula limits for zeolites are not met. (2) There is a large variability in measured cation contents from particle to particle from the same source as well as substantial differences in average compositions from different sources. However, sedimentary erionites cannot be termed a separate mineral species because the crystallographic data are consistent with erionite and new zeolite names cannot be proposed on the basis of Si:Al ratios alone. In addition to chemical differences between erionite from different sources, there are also morphological differences. By analogy with asbestos minerals, differences in composition and morphology may have implications for relative toxicity, and future research should include consideration of these aspects.

Keywords: Analysis, chemical (mineral), erionite, electron microscopy, medical mineralogy, zeolites

INTRODUCTION

Erionite is a naturally occurring mineral that belongs to a group of silicate minerals called zeolites. It was originally described from the Durkee opal mine near Durkee, Baker County, Oregon, and named by Eakle (1898). The name was derived from a Greek word that means wool because at the type locality the erionite occurs as white, wool-like fibers. However, this is an uncommon habit, which has also been observed in the Reese River zeolite deposits, near Austin, Nevada (Gude and Sheppard 1981), but not elsewhere. For more than half a century, this zeolite was considered extremely rare, and no additional occurrences were listed until Deffeyes (1959) described material from Nevada and Wyoming. Unlike the type erionite, these subsequent occurrences were either crystals formed in the vesicles of (mainly) basaltic lavas, or microscopic acicular-to-fibrous crystals in diagenetically altered, silicic, vitric tuffs of Cenozoic lacustrine deposits (Mumpton and Ormsby 1976). In most cases the erionite is likely to be a later, pore-filling, re-crystallization of dissolved volcanic glass. Numerous additional discoveries of erionite have been reported throughout the world, for example

* Present address: Zefon International, Inc , 5350 SW 1st Ln, Ocala, FL 34744, U.S.A. E-mail: mharper@zefon.com

0003-004X/17/0008–1718$05.00/DOI http //dx doi org/10 2138/am-2017-6069

in many localities within the western U.S.A. (Van Gosen et al. 2013). The large crystals found in the vesicles of mafic volcanic rocks have been the materials most commonly examined when researching the crystallography and composition of erionite. The standard published formula for erionite is $Al_{10}Si_{26}$, which gives a Si:Al wt% ratio of 2.7 (mol% ratio of 2.6). The average wt% value for the 25 different erionites analyzed by Passaglia et al. (1998), all of which came from vesicles in volcanic rocks, using electron probe microanalysis (EPMA) was 2.6 (range 2.1–3.7). However, there are differences in major element (Si, Al) chemistry between erionites from the two geological settings (vesicles in lavas and "sedimentary" deposits), and this was noted by Gude and Sheppard (1981). An examination of Figure 1 in Sheppard (1996) shows little overlap in the Si:Al ratio between erionites from these two sources. Figure 1 of Sheppard (1996) also shows most sedimentary erionites having Si:Al ratios greater than 3.3, up to around 3.8.

Erionite occurring in the "sedimentary" formations crystallizes as needle-like fibers of nanometer- to micrometer-size widths. Larger bundles of these crystals are also common, often with a splayed appearance. Disturbance of the friable rocks containing these microscopic crystals can generate airborne fibers with physical dimensions similar to asbestos fibers. These particles may further resemble particles of asbestos by exhibiting similar toxicity. For example, it has long been known that residents of some Turkish villages where erionite-containing rock was used to construct homes have a remarkably high risk for development of malignant mesothelioma (Baris et al. 1978; Rohl et al. 1982; Simonato et al. 1989; Baris 1991; Carbone et al. 2011). However, it should be noted that an early field survey by Mumpton (1979) urged caution in the attribution:

> In so far as a positive correlation between the occurrence of erionite or other zeolites in the tuffs from these Turkish villages and the incidence of pleural mesothelioma, the data are equivocal, and tend to suggest that no correlation exists.

The possibility exists that differences in chemistry and morphology of erionite found in different areas may have consequences for toxicity.

Procedures are needed to identify erionite fibers in bulk rock, soil, and air samples to assess the potential for exposure and these procedures likely will include chemical analyses. In addition, an understanding of the morphology and major and minor element chemistry of these particles is necessary for the determination of factors that influence toxicity. Therefore, it is important that investigators be aware of the differences between sedimentary erionite and the more classic crystals most often described in the literature. However, the determination of chemistry of these microscopic crystals requires great care. Previous analyses reported in the literature (Dogan and Dogan 2008) appeared to meet the Mg% requirement for erionite and the zeolite cation balance error formula, using the typical limitation (E < 10%). After recomputing, the reported analyses were found to be in error. A more recent publication (Dogan 2012) indicated "Among the 60 analyses ... only 3 passed both E% and Mg-content tests (5.0%). This shows difficulty of quantitative characterization of the erionite series minerals." A publication from the U.S. Geological Survey (USGS) used a wider criterion for the balance error (E < 20%) to account for the obviously increased variance in the analyzed cation contents (Lowers et al. 2010).

Prior to this study we had submitted fractions of the Rome, Oregon, tuff to different commercial laboratories for comparative analyses of fiber-like particles by TEM-EDS and SEM-EDS. However, very little consistency was observed between laboratories. Some laboratories did not report important elements (e.g., Na, Mg, Fe), giving as the reason that these elements were not observed above their limit of detection, and one laboratory consistently reported high Fe in all samples. It became clear that higher energies associated with TEM caused severe disruption to erionite crystals, resulting in physical distortion (Fig. 1), rapid loss of diffraction pattern, and a loss of "volatile" elements such as Na. Depletion of alkali ions from glass under EPMA by migration to an electron-rich space charge layer has been studied and corrections described for this phenomenon (Nielsen and Sigurdsson 1981). A similar effect was proposed for the loss of Na in the analysis of the zeolite, clinoptilolite, even after precautions against loss had been taken (Broxton et al. 1987). Electron beam damage under electron microscopy is also a well-known phenomenon, for example causing broadening and weakening of diffraction spots in chrysotile (Zusmann and Brindley 1957) and

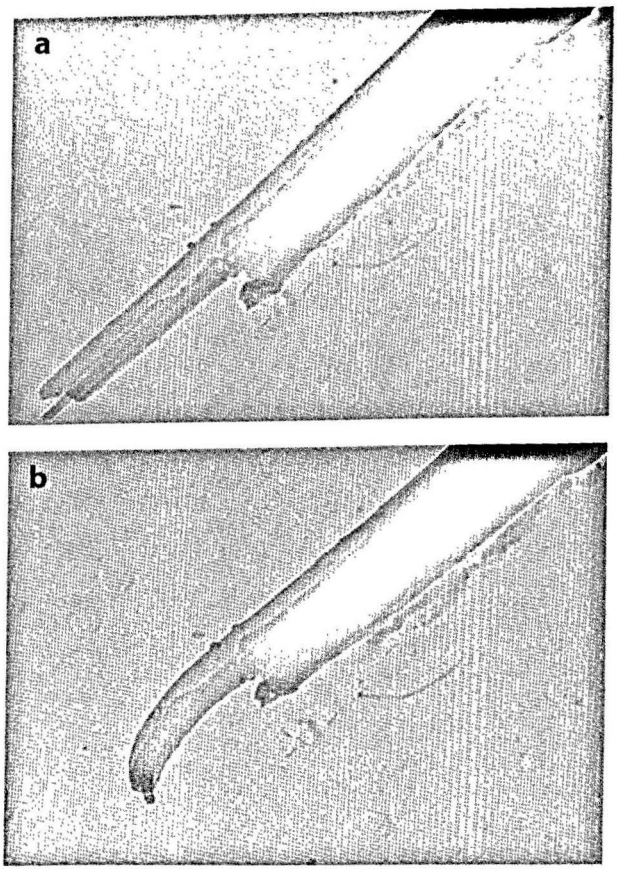

FIGURE 1. Distortion of an erionite crystal with increasing time under 100 keV TEM beam energy. Photographs courtesy of IATL. (**a**) With beam first applied. Scale: particle is approximately 300 nm wide at thickest point. (**b**) Same particle after collection of diffraction data.

charging and breakage of illite fibers (Purvis 1991). Thus there is a conflict between the high current and beam dose preferred to produce bright images and the lower beam doses necessary to produce good diffraction patterns (Steel and Small 1985). Just recently beam damage has also been observed for relatively robust structures, such as amphibole asbestos (Martin et al. 2016). There are three major mechanisms of beam damage, known as knock-on interaction ("sputtering") through elastic scattering (the same mechanism that results in diffraction patterns), radiolysis, which is due to ionization through inelastic scattering (the same mechanism that gives rise to EDS analyses), and electrostatic charging, although in many cases the last two mechanisms cannot be distinguished, especially in the case of a highly intense and focused electron probe (Jiang and Spence 2012). The damage mechanisms have been studied to some extent in zeolites. A study of the zeolite MCM-22 indicated that radiolysis dominates at low energies (<70 keV), and the damage depends on the dose rate above a threshold irrespective of time of exposure, whereas at higher energies sputtering also occurs and there is no threshold dose rate, the damage being a consequence of total dose, i.e., dose rate times time of exposure (Ugurlu et al. 2011). Since most TEM analyses are conducted at energies around 100 keV or higher, both mechanisms are probably occurring.

In this work we confirm by selected area X-ray diffraction (SAED) of individual crystals that the minerals we are examining are zeolites, specifically erionite. We present analyses of large numbers of crystals by energy-dispersive spectroscopy (EDS) using transmission electron microscopy (TEM), with comparison to analyses by electron microprobe with wavelength-dispersive spectroscopy (WDS). TEM-EDS systems are readily available in many laboratories for commercial use; although electron microprobe analyses are considered to be quite accurate when the analysis is performed properly, these instruments are not common in industrial hygiene laboratories, and air-sample filters from hygienic investigations are most likely to be analyzed by TEM, with EDS (and SAED). Finally, we also present field emission-scanning electron microscopy (FE-SEM) and high-resolution TEM (HR-TEM) micrographs to illustrate the range of morphology in crystals from different locations.

MATERIALS

Five samples of volcaniclastic sedimentary rock were obtained from various locations, primarily from the western U.S. The material designated Rome was collected by the primary author in the vicinity of the "Pillars of Rome," near Rome, Oregon. Material was selected from a specific horizon that contained ~75% fibrous crystals by visual area estimation using a field optical microscope to examine the samples. This was subsequently examined in the laboratory using confocal focusing techniques to evaluate the three-dimensional geometry of all constituent particles in the tuff. The non-erionite material was almost entirely volcanic glass. From the geometry of the different particles and assumed densities for erionite and glass, the sample was determined to consist ~35% fibrous crystals by weight. This material is now available in 10 g aliquots for research purposes from RTI International (Research Triangle Park, North Carolina[1]). The material designated CGNF was collected by the primary author from the Arikaree Formation of Palaeogene (Miocene-Oligocene) age from Reva Gap in the Slim Buttes Land Unit of the Sioux Ranger District of the Custer-Gallatin National Forest, South Dakota. This material contained ~35% fibrous crystals by visual area estimation and using the same technique to convert from area to mass as was used on the Rome material, ~1% by weight. Sub-samples of this material can also be provided through contact with the primary author.

[1] Contact: Todd Ennis, jte@RTI.org.

The material designated Killdeer was collected from the slope of South Killdeer Mountain, Dunn Co., North Dakota. (Saini-Eidukat and Triplett 2014) It is located approximately 75 miles from the Slim Buttes Land Unit and is also believed to be from the Arikaree Formation. Area and weight percentages of fibrous crystals were not determined for these samples, which are not available for further distribution. A small quantity of a material designated Karain, from Cappadocia, Turkey, was provided by International Asbestos Testing Laboratories (IATL, Mt. Laurel, New Jersey, U.S.A.). The material designated Reese River was collected by the primary author from the Reese River zeolite deposit, Lander Co., Nevada (Gude and Sheppard 1981). The erionite is reported to fills joints in gray to brownish-gray lacustrine mudstone of probably Pliocene age. However, there is currently no outcrop and the material used in this work was collected from the float in the indicated area of occurrence. It has the appearance of paper scraps, which are clearly fibrous when broken. It is 100% erionite, with the same wooly appearance under the optical microscope as that from Durkee, Oregon; these are the only two locations known where this particular habit occurs in quantity. Macroscopic crystals of erionite were extracted from vesicles in a sample of volcanic rock labeled "Ajo well #1 or Phelps Dodge Corporation Well #1, Ajo, Pima Co., AZ" from the primary authors collection for comparison purposes. These were submitted for EPMA, but insufficient sample was available for TEM-EDS, XRD, or SAED analysis.

Methods and results: SAED

For the SAED analyses, each sample was initially lightly ground in a mortar and pestle. The resulting fine mineral powder was placed in a centrifuge tube and suspended with reagent alcohol (VWR Analytical). The suspension was pipetted onto carbon-coated 200 mesh copper TEM grids. Analysis was conducted using a JEOL 1200 EXII transmission electron microscope (TEM) operated at 100 keV and equipped with an IXRF Iridium EDXA and AMT side mount digital camera The electron beam's intensity has been shown to rapidly decay the crystal lattice of zeolites. Therefore, the TEM grids were mounted in a Gatan liquid nitrogen cooled double tilt TEM specimen holder. This holder keeps the sample at –170 °C and helps to minimize the beam's impact on the crystal lattice thus preserving the diffraction pattern for imaging and crystal zone indexing. From the diffraction patterns obtained, indexing measurements were performed using the AMT software application to determine the miller indices and zone axes. All fibers examined, including all 20 fibers in the first analysis from the bulk CGNF sample, gave patterns consistent with erionite, however occasional fibers in this sample could also be found with patterns indicating the possibility of an intergrowth with another mineral, this finding is discussed in more detail under morphology. Variations were noted in the patterns between erionites from different sources as shown in Figure 2. Killdeer patterns were weak and did not last long. Karain patterns were not as difficult to obtain as ND patterns, but were not as clear as those from Rome, CGNF or Reese River Finally, a CGNF sample was treated with 1:1 (50%) HCl and fibers under TEM showed no discernable SAED patterns and also very little Al remaining under EDS.

Methods: EPMA

Seven samples of "sedimentary" erionite (Rome; CNF; Killdeer 3-01, 3-02, and 3-03; Karain; and Reese River) together with the vesicular erionite from Ajo, and National Institute of Standards and Technology (NIST) reference zeolites were submitted for microprobe analysis at the University of Oregon. Compositional analyses were acquired on an electron microprobe (Cameca SX100) equipped with five tunable wavelength-dispersive spectrometers and a 40° takeoff angle. A focused beam with an energy of 15 keV and current of 10 nA was used. Elements were acquired (all $K\alpha$ lines) using an LiF analyzing crystal for Fe, an LPET crystal for K and Ca, a TAP crystal for Na and Al, and an LTAP crystal for Si and Mg. The standards utilized were synthetic MgO for Mg, synthetic SiO_2 for Si, NBS K-412 mineral glass for Al and Fe, chlorapatite (halogen corrected) for Ca, nepheline for Na, and orthoclase for K. The on-peak counting times were 40 s for K; 90 s for Si, Mg, and Ca; and 120 s for Na, Al, and Fe. The off-peak correction method for K was linear with a counting time of 40 s; Na, Al, Fe, Si, Mg, and Ca were background corrected using mean atomic number (MAN) intensity data that were calibrated and continuum absorption corrected. Count intensities were corrected for deadtime and standards were also corrected for any drift in intensity over time. A time-dependent intensity (TDI) drift correction was used for Na and K to account for any loss over time (Nielsen and Sigurdsson 1981); both elements were first tested to ensure their concentrations did not steeply drop off during the assigned analysis time interval to avoid having an exponential fit to the TDI data. ZAF or Phi-Rho-Z matrix corrections (Armstrong-Love/Scott algorithm; Armstrong 1988) and the LINEMU mass absorption coefficients data set (Henke 1985) were utilized. Oxygen was calculated by cation stoichiometry and included in

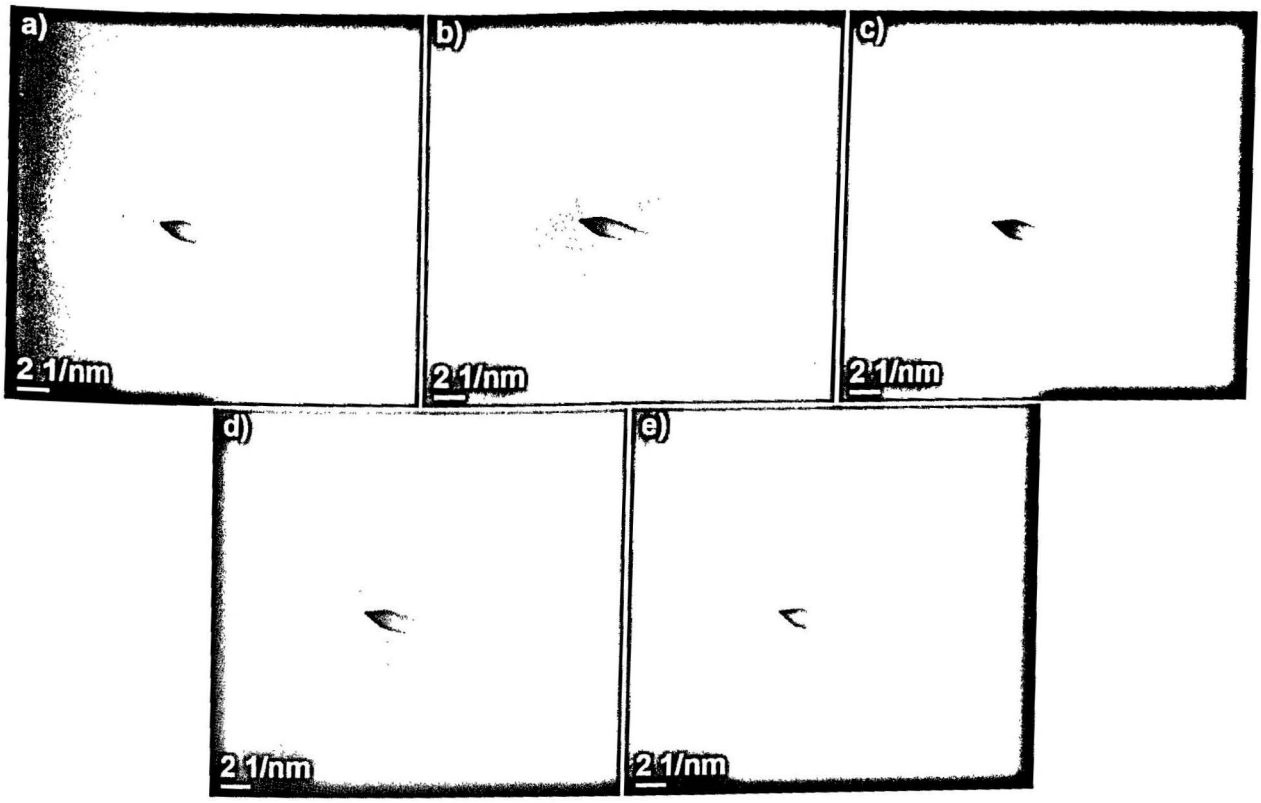

FIGURE 2. SAED of erionite particles. (**a**) Rome, Oregon. (**b**) CGNF, South Dakota. (**c**) Killdeer 03-03, North Dakota. (**d**) Karain, Turkey. (**e**) Reese River, Nevada.

the matrix correction. Particles were selected for analysis on the basis of having the appearance of fibers (aspect ratio >3:1) and being at least 5 μm long, although actual size measurements were not made. A trigonal prism particle correction (for curved top and flat sides or fiber-shaped materials), assuming a width of 1 μm, was used The choice of width did not affect elemental ratios or range of variability. Elemental analyses were normalized to 100% assuming no hydration water. Approximately 20 particles were analyzed in each sample.

As the EPMA microscope did not include SAED, particles resembling fibers (aspect ratio > ~3:1, length > ~5 μm) in the sedimentary zeolites were specially selected for these analyses. These were most likely to be erionite, as confirmed by the separate SAED analyses. Occasionally, glass, clay minerals, or gypsum may appear as fibers under the microscope, however, their composition would be very different from erionite. The NIST zeolite A reference material 8851 was used to test the analytical system. NIST 8851 has a 50% particle diameter of 2.24 μm measured by laser light scattering, which is similar to the size of the sedimentary erionite particles, and had a similar response to the erionite particles during analysis of Na. NIST zeolite Y reference material 8850 was also examined. Results shown in Table 1.

Methods: TEM-EDS

The analyses reported here used a 200 keV JEOL 2100F scanning transmission electron microscope (STEM) with an Oxford Inca EDS attachment located at the NIOSH Alice Hamilton Laboratory in Cincinnati, Ohio. The TEM-EDS systems limit of detection is considered to be two or three times the background level, which usually will translate to 2–4 wt% composition depending on the energy and

TABLE 1. EPMA analyses (elemental wt%, dry weight basis) of fibers from rock samples

	Si				Al				Mg			Fe		
	Low	High	Median	CV%	Low	High	Median	CV%	Low	High	Median	Low	High	Median
Karain (n = 19)	30	36	34	6.0	6.4	10	8.9	12	0.51	2.5	0.77	0.16	6.2	0.34
Rome (17)	25	36	32	10	6.9	11	7.9	13	0.12	3.9	1.0	0.48	7.1	1.4
ND 03-01 (10)	29	36	34	6.8	6.1	14	8.9	30	0.19	3.5	0.87	0.16	4.6	0.27
ND 03-02 (16)	33	37	35	2.9	6.8	10	8.3	13	0.17	1.7	0.59	0.10	1.3	0.14
ND 03-03 (11)	30	39	36	6.9	6.9	13	9.0	22	0.10	1.0	0.66	0.08	0.42	0.17
CGNF (19)	24	37	34	11	6.7	13	8.3	17	0.58	2.7	1.2	0.27	3.0	0.55
Reese River (17)	26	36	33	7.7	6.6	13	9.5	14	0.18	2.0	0.27	0.11	4.9	0.44

	Na			K			Ca		
	Low	High	Median	Low	High	Median	Low	High	Median
Karain (n = 19)	0.75	4.8	1.8	2.7	4.6	3.6	1.1	2.8	1.4
Rome (17)	0.25	4.6	0.54	1.5	5.9	4.4	0.61	7.3	4.5
ND 03-01 (10)	0.1	1.7	0.3	2.3	5.0	3.2	1.1	4.5	2.0
ND 03-02 (16)	0.02	1.3	0.07	1.9	3.7	2.7	2.6	3.8	3.3
ND 03-03 (11)	0.1	0.6	0.34	0.03	4.0	2.5	0.01	3.4	2.4
CGNF (19)	0	5.1	0.87	1.0	4.4	3.1	1.3	11	1.8
Reese River (17)	0.16	0.55	0.25	1.5	6.5	3.1	2.0	7.8	4.0

Notes: Sample numbers refer to horizons in Saini-Eidukat and Triplett (2014). ND = Killdeer. CV = coefficient of variation.

noise level. Thus it can be quite difficult to obtain precise and accurate analyses of elements at <1 wt%. Most, but not all of the same samples analyzed by EPMA were also submitted for TEM-EDS. The NIST zeolite reference material 8851 was used to test the EDS system and determine the microscope conditions necessary to limit electron beam exposure such that sodium in the reference material (7.225 ± 0.094% assuming full hydration; by X-ray fluorescence spectroscopy and instrumental neutron activation analysis) was not affected. This reference material was considered by the analyst to have a similar beam sensitivity to Na as erionite. Operating the TEM in the scanning transmission mode using the smallest 0 2 nm probe available with the 25 μm condenser aperture gave the most comparable analysis of Na to the reference composition in 8851. The sample was tilted 10° toward the EDS detector to increase counts to obtain a satisfactory signal-to-noise ratio with a 100 s live count. NIST 8850 was also used as a reference. It has a similar particle diameter to NIST 8851, but a lower content of Na. The EDS data were processed with OXFORD software; GATAN software did not produce as close a match to the reference material composition. Elemental analyses were normalized to 100% assuming no hydration water. For comparison with NIST reference compositions, the NIST analyses were also normalized to 100% without water of hydration.

Ten fibers from each of the Rome, CGNF, and Karain (Turkey) samples were analyzed using this procedure ("Old TEM" data in Table 2). Subsequently, comparison with the EPMA data suggested that the EDS K percentage tended to be low, even though Na was unaffected. Repeat analyses of the Rome and CGNF samples were performed where beam exposure was further reduced by limiting the magnification to under 150 000× and by analyzing fibers ≥150 nm in diameter. Thirty Rome fibers, and 30 CGNF fibers from a sample sieved through screens designed to pass particles <15 μm diameter (five removed for Si >40 wt%, but this did not affect the median ratio of Si:Al), were analyzed using the new conditions and agreement with the microprobe data improved greatly ("New TEM" in Table 2).

Results of chemical analyses

Under EPMA, the average of 20 particles of NIST 8851 gave Si: 20 wt% (expected 20%); Al: 19% (expected 19%); Na 15% (expected 16%). The coefficients of variation (CV) were 11% for Si, 17% for Al, and 20% for Na. The average of 20 particles from NIST 8850 were Si: 31% (expected 30%); Al: 12% (expected 12%) and Na: 6.9% (expected 9.7%); the CV's were 5.9% for Si, 3.6% for Al, and 13% for Na. The average of 10 particles from NIST 8851 analyzed under the optimized TEM-EDS conditions gave Si: 23 wt% (expected 20%); Al: 22% (expected 19%); Na 15% (expected 16%). The coefficients of variation (CV) were 11% for Si and Al, and 5.9% for Na. The average of 5 particles from NIST 8850 were Si: 34% (expected 30%); Al: 12% (expected 12%) and Na: 9.2% (expected 9.7%); the CV's were 2.8% for Si, 3.6% for Al, and 6.5% for Na.

The EPMA results from the sedimentary erionite samples are shown in Table 1. A very few individual analyses were removed when calculating mean, median, and standard deviation. Not removing these analyses hardly affects the values, but by excluding those few analyses we feel the values are a more accurate representation of the mean and median of the whole population. The number of analysis points used is given in the table; the number not included were Rome (0); CNF (1); Killdeer 03-01 (8), 03-02 (4), 03–03 (4); Karain (0), Austin (0). Most of the data removed from consideration had very low Al contents (<6 wt%), except for one sample from CGNF (Si >40 wt%), two from Killdeer 03-01 (one with Fe >8 wt% and one with Ca >12 wt%), and one from Killdeer 03-02 (Al >15 wt%). Under the TEM it is possible to observe some fibers are associated with smaller particles on their surface. The observational capability of the TEM usually allows these particles to be avoided in the analysis, but it is more difficult do so in the microprobe. Therefore it is possible that some of the outlier chemistries are the result of including associated particles in the analysis, for example, quartz (high Si), illite clay (high Fe), or calcite (high Ca).

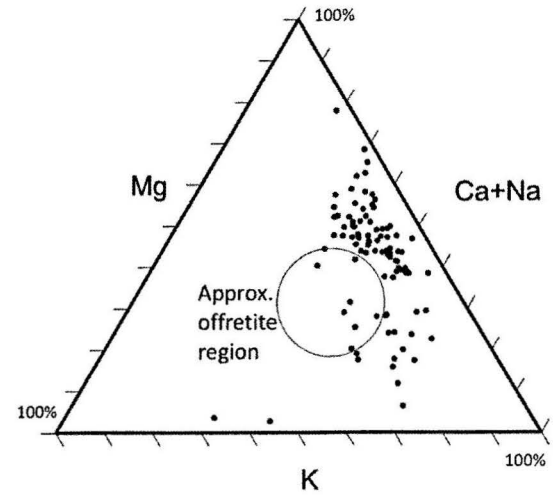

Figure 3. Ternary plot of all erionite analyses (circle is approximate compositional field for offretite; Passaglia et al. 1998).

The Mg content of all these samples is low. A ternary plot (Fig. 3) indicates that the majority of analyses plot outside of the compositional field considered applicable to offretite. Table 2 provides a comparison between EPMA and TEM-EDS of some useful metrics: Si/Al ratio, O wt% and cation wt%. Note that these analyses, reported in wt% on a dry weight basis (assuming no water of hydration) should not be compared directly with published analyses that have assumed (or in some cases, measured) water of hydration. Repeat analysis of the Rome and CGNF samples with the additional restrictions noted (designated new TEM) gave almost identical results under TEM-EDS to EPMA.

Discussion of chemical analyses

The NIST 8851 samples results are very comparable to the reference values using either EPMA or TEM-EDS and the CV's are never greater than 20% and typically 12% or less. The CV's for TEM-EDS are generally tighter than those with EPMA. The Pima Co. erionite under EPMA gave a Si:Al ratio of 2.66, as expected for an erionite from a vesicular lava. Negligible Na was present but the mean content of Ca was 4.2% and the mean content of K 3.4%, both comparable to mean Ca and K percentages in many of the sedimentary erionites analyzed. However,

Table 2. Median values of Si:Al ratios and elemental wt% compositions (dry weight basis) from different analytical techniques

	Si:Al ratio		O wt%		Ca wt%		K wt%		Na wt%	
	Microprobe	TEM	Microprobe	TEM	Microprobe	TEM	Microprobe	TEM	Microprobe	TEM
Rome (microprobe17/Old TEM10)	3.9	4.0	48	51	4.5	3.2	4.4	1.9	0.4	0
Rome New TEM (30)		4.0		45		3.4		4.3		0
CGNF (microprobe19/Old TEM10)	3.9	4.0	49	52	1.8	1.3	3.1	1.7	0.9	0.4
CGNF New TEM (24)		3.9		47		1.5		3.8		0.9
Karain (microprobe19/Old TEM11)	3.8	3.4	49	43	1.4	1.1	3.6	4.7	1.8	1.9

the CV's of Ca and K determinations in the Pima Co. sample (Ca 16%, K 15%) were comparable to those of Na in the NIST reference materials and generally much smaller than for the equivalent analyses of cations in the sedimentary erionites, which ranged for most between 30 and 100%.

The Reese River sample and the Turkish sample had Si:Al ratios, which, while high, are still within the range reported previously for sedimentary erionites. However, there is a consistently higher Si:Al ratio, 3.9–4.0, in the other samples (Killdeer 03-01 samples, not listed in Table 2, also had a median Si:Al ratio of 4.0), which is indicative of a unit cell of Al_6Si_{30}, rather than the classic unit cell of $Al_{10}Si_{26}$. Hay (1964) noted that pH exerts a strong control over the silica content of crystallizing zeolites, with an inverse correlation between the two. The smaller substitution of Si by Al in the structure of the erionites from these localities requires fewer extra-framework cations for balance. Even so, none of these analyses meet the cation charge balance error formula limits. Hydrogen ions compete with base cations (Hay 1966, p. 78) and this competition may be enhanced at the lower pH of high-silica zeolite formation. The extra-framework cation content also varies between localities, with the Rome sample having the highest content. Finally, an extreme (order of magnitude) variation in any cation can be found between two fibers in the same sample. The consistent picture between TEM-EDS and EPMA of low extra-framework cation content and high variability does not appear to be related to a problem with the analytical techniques. A possible geological explanation for these observations is very local ion-exchange equilibria interactions with groundwater and possibly also other minerals within the rock. Broxton et al. (1987) detailed variations in alkali and alkaline earth cation composition of clinoptilolite over the geographical area they examined, and attributed the variation to mobilization during diagenesis (i.e., formation of zeolite from volcanic glass), but they did not observe variation on the microscale noted here. However, they only reported analyses that met the cation balance equation, discounting others.

We believe the new TEM-EDS results have sufficient precision using the stated microscope conditions that TEM-EDS systems can be used in the future to test for erionite presence, especially in combination with other analytical methods such as SAED patterns obtained under low-temperature conditions, provided similar quality systems to those described here are employed to ensure the accuracy of analyses. Prior published analyses of erionite in these kinds of samples by TEM-EDS should be treated with extreme caution, especially as there is no possibility of confirming them against an orthogonal technique, such as inductively coupled-plasma optical-emission spectroscopy, when the microscopic crystals make up only a few percent of the rock. This data set suggest that differentiation between K-, Na-, and Ca-erionites is not possible for the sedimentary erionites studied because of the cation content variation within single samples.

It is interesting to note the large proportion of low-Al particles in the Killdeer samples compared with the others. This difference in chemistry is not the result of analyzing other zeolites by mistake as no other zeolites were identified by XRD in the bulk samples (Saini-Eidukat and Triplett 2014 and current data). In addition, the SAED patterns of Killdeer samples are typically very blurred compared to the patterns from other samples. It should also be noted that loss of diffraction pattern and loss of Al was apparent in our acidified sample of CGNF, suggesting that these Killdeer samples may have been subjected to acidic groundwater at some point in their geological history (although we do not propose that acidification after crystallization is the reason for the generally high Si:Al ratios in these samples). This finding may have some bearing on the extra-framework cation contents of the minerals studied. In laboratory studies of the cation-exchange capacity of other zeolites, Hoss and Roy (1960) noted:

> The data ... bring out the surprising fact that in many cases the cations do not appear to balance the charge generated by Al^{3+} replacement of Si^{4+}... [while] Hydronium substitution in such samples could not be proved conclusively ... Hydronium substitution is believed to take place easily ... Cation deficiency in natural zeolites can be explained in the same way.

However, it is the case that experimental proof for such a hypothesis is lacking, and none is offered here.

Another interesting component of the chemistry is iron. In the CGNF samples, Killdeer and Reese River samples Fe is very low, typically less than 0.25%. However, by EPMA, 35% of Rome particles had >2% Fe. Although this finding was not reproduced in our TEM-EDS analyses, it was also noted by Matassa et al. (2015) in their analysis of Rome material. It is possible that this additional Fe is external to the crystal as has been noted previously (Ballirano et al. 2009), and it may have been included in the wider beam of our EPMA analyses. As noted above, particles adhering to the fibers were observed under TEM and every effort was made to exclude them from the analysis and this may be why the Fe content appears lower under our TEM analysis. The existence and location of Fe in these particles may be important as it has been hypothesized that Fe may be a factor in the toxicity of erionite (Croce et al. 2015).

Morphology under field emission SEM and high-resolution TEM

For analysis by field emission (FE) SEM, particles were suspended in distilled water and filtered through a 0.2 μm Nucleopore filter. The filters were trimmed and placed on an aluminum stub with double-stick carbon tape and sputter-coated with gold-palladium and imaged with a, using a Hitachi S-4800 FE-SEM operated at 5 kV. Samples were also imaged with high-resolution (HR) TEM, using a FEI Tecnai G2 Twin TEM at an accelerating voltage of 200 kV. Figure 4 shows FE-SEM images of individual nano-fibrils around 40–60 nm wide, which were found in all samples and appear very similar. However, the majority of fibers are much wider than these. In some case, this can be seen to be because the fibers are bundles of thin fibrils, but this is not always the case. Figure 5 shows HR-TEM images of Rome erionite side-by-side with CGNF erionite with contrasting morphologies. The Rome erionite particle is clearly a bundle of the nano-width fibrils and the CGNF particle is a twisted ribbon-like blade ~150 nm wide with no clear bundling of finer fibrils. Although as noted, individual nano-width fibrils

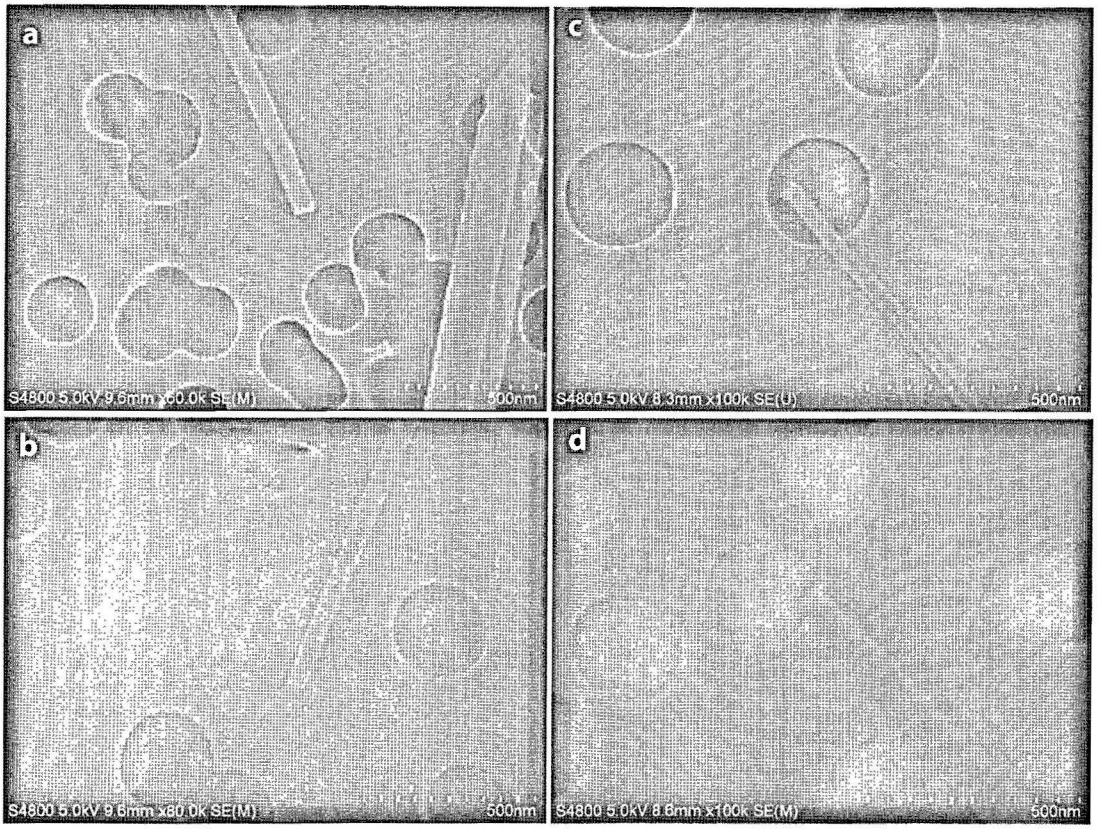

FIGURE 4. FE-SEM images of individual erionite fibrils from different samples: (**a**) Rome, (**b**) CGNF, (**c**) Karain, and (**d**) Killdeer.

can be found in all samples, most of the CGNF particles more closely resemble the ribbon-like blades, while most of the Rome particles appear as bundles. The morphology of the CGNF fibers may be consistent with our diffraction data. Matassa et al. (2015) identified and measured two different *d*-spacings in their sample of erionite from Durkee, Oregon, one perpendicular to the long axis of the fiber and one parallel to the fiber elongation corresponding to $d_{002} = 0.747$ nm, and noted that the fibers they

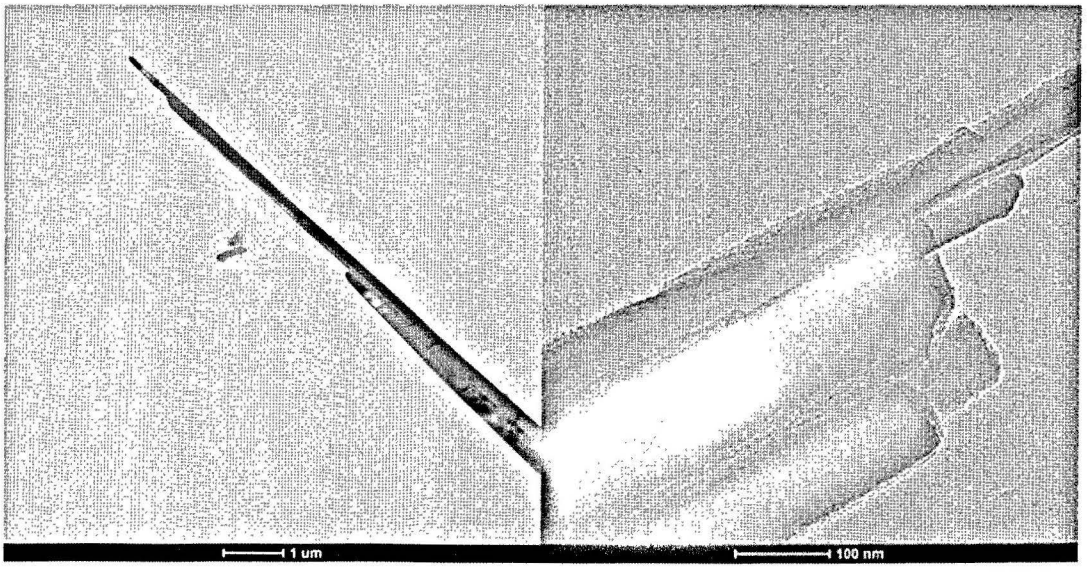

FIGURE 5. HR-TEM images of CGNF and Rome fibers side-by-side (note difference in scale). (**a**) CGNF, (**b**) Rome.

FIGURE 6. "Wooly" erionite from Reese River, Nevada (FE-SEM).

observed also presented as ribbons. Thus the different spacing may be only an artifact of fiber position, rather than an intergrowth with another mineral; unfortunately it was not possible to tilt our stage to investigate this further.

Additional differences between samples from different locations were apparent with a change in scale. Under lower magnification, for example, CGNF erionite particles (fibers) are generally observed to be longer (median 7 vs. 5 μm) and wider (0.4 vs. 0.3 μm) than Rome fibers, but with similar aspect ratio (approx. 20:1), although the Rome sample often shows many short (~1 μm) fibers. The Karain, Turkey, sample is generally comprised of thinner fibers (~0.15 μm) as also noted by Lowers et al. (2010) and the Reese River sample is comprised of large bundles of nano-fibrils with a very wavy appearance (Fig. 6). The critical health outcome from exposure to airborne erionite is mesothelioma. In asbestos-related disease, lung cancer occurs in association with mesothelioma, but that is not the case with erionite. It is not known whether difference in particle sizes and morphologies between asbestos and erionite, and between erionites from different locations effects health outcomes following exposure, but it may be so, and further research is required, which should include a fuller analysis of mineral properties, as, for example, in Mattioli et al. (2016).

DISCUSSION

After careful analyses by microprobe-WDS and TEM-EDS, we agree with Dogan (2012) that the analysis of erionite by TEM-EDS is difficult, but it can be optimized for identification and analysis. First, the EDS should be calibrated on NIST 8851 and/or 8850. Magnification should be kept below 150 000× and particles analyzed should be wider than 150 nm. The beam should be the narrowest available and dwell time must be limited. A minimum of 30 erionite particles should be studied per sample by either TEM-EDS or EPMA to account for compositional variations between particles. Even with careful consideration of these analytical parameters, we believe it is not possible to classify the erionites we have studied from volcaniclastic sedimentary rocks as Na-, K-, or Ca-erionites because of the large range of compositions between individual crystals. Macroscopic crystals of erionite formed in magmatic vesicles match the "ideal" formula for erionite, but erionite crystals from volcaniclastic sedimentary environments do not, being first poorer in aluminum, so requiring fewer extra-framework cations for balance, and second being further depleted in cations over the number necessary to meet the charge balance error formula (it is possible that the balance may be obtained through hydrogen ions, although this was not studied). We believe these chemical differences to be a real reflection of either different formational micro-environments or differences in the later diagenetic processes operating on a microscale, but we do not believe it is because of uncertainty in the analytical techniques, since the variation in the cation content from crystal to crystal is much greater than the analytical precision we have confirmed using reference materials. Since the chemistry is so variable, SAED is a valuable technique for more defensible erionite identification when other zeolite minerals could be present and a cryogenically cooled stage makes it possible to obtain these. The X-ray diffraction patterns of the minerals we have studied here are consistent with erionite and the International Mineralogical Association does not recognize new zeolite species on the basis of Si:Al ratio alone (Coombs et al. 1997). Thus the analyses we present here, while unusual, cannot be construed to indicate a new mineral. In addition to variations in chemistry within and between samples, there are considerable variations in morphology. This variation in chemistry and morphology between samples from different locations may have a bearing on relative toxicity, and this should be investigated further.

IMPLICATIONS

Erionite occurs in volcaniclastic rocks and soils; in some villages in Turkey the presence of erionite in local rocks is associated with mesothelioma, a disease also associated with inhalation of airborne asbestos. Since volcaniclastic rocks containing erionite are widely present in the western U.S.A., there is a concern over potential health issues following inhalation of dust particles in these areas and thus there is a need to identify and quantify erionite particles found in air samples during hygienic investigations. Previous attempts to analyze the few micrometer-sized erionite particles found on air sample filters under transmission electron microscope (TEM) encountered difficulties due to electron beam damage. Recommendations are presented for accurate analysis by both energy-dispersive spectroscopy (EDS) and selected-area electron diffraction (SAED) and these recommendations will be incorporated into consensus standard methods under development. In addition, our analytical findings have implications for current and future studies on the toxicity of erionite. Differences in the relative toxicity of asbestos minerals have been related to variations in composition and morphology. It is possible that the variation in volcaniclastic erionite composition and morphology between localities we have found may have an analogous bearing on toxicity, and this should be investigated further. The major differences between erionites from magmatic vesicles and those that have crystallized in volcaniclastic sedimentary rocks needs to be fully recognized. Furthermore, the particle-to-particle variation in cation chemistry has implications for the interpretation of prior studies that have examined few, or only single, particles.

ACKNOWLEDGMENTS

The authors thank Diane Schwegler-Berry (NIOSH) for Figures 4 and 6, Stacy Doorn (RTI) using Duke University equipment for Figure 5, International Asbestos Testing Laboratories (IATL) for Figure 1, and the colleagues who assisted in field specimen collections. EPMA analyses (Julie Chouinard) were provided for-fee from NIOSH.

Disclaimer: The findings and conclusion in this report are those of the author(s) and do not necessarily represent the official position of the National Institute for Occupational Safety and Health.

REFERENCES CITED

Armstrong, J.T. (1988) Quantitative analysis of silicates and oxide minerals: Comparison of Monte-Carlo, ZAF and Phi-Rho-Z procedures. Microbeam Analysis, 239–246.

Ballirano, P., Andreozzi, G.B., Dogan, M., and Dogan, A.U. (2009) Crystal structure and iron topochemistry of erionite-K from Rome, Oregon, U.S.A. American Mineralogist, 94, 1262–1270.

Baris, Y.I. (1991) Fibrous zeolite (erionite)-related diseases in Turkey. American Journal of Industrial Medicine, 19, 374–378.

Baris, Y.I., Sahin, A.A., Ozesmi, M., Kerse, I., Ozen, E., Kolacan, B., Alinörs, M., and Göktepeli, A. (1978) An outbreak of pleural mesothelioma and chronic fibrosing pleurisy in the village of Karain/Urgup in Anatolia. Thorax, 33, 181–192.

Broxton, D.E., Bish, D.L., and Warren, R.G. (1987) Distribution and chemistry of diagenetic minerals at Yucca Mountain, Nye County, Nevada. Clays and Clay Minerals, 35, 89–110.

Carbone, M., Baris, Y.I., Bertino, P., Brass, B., Comertpay, S., Dogan, A.U., Gaudino, G., Jube, S., Kanodia, S., Partridge, C.R., and others. (2011) Erionite exposure in North Dakota and Turkish villages with mesothelioma. Proceedings of the National Academy of Sciences, 108, 13,618–13,623.

Coombs, D.S., Alberti, A., Armbruster, T., Collela, C., Galli, E., Grice, J.D., Liebau, F., Mandarino, J.A., Minato, H., Nickel, E.H., and others. (1997) Recommended nomenclature for zeolite minerals: report of the subcommittee on zeolites of the international mineralogical association, commission on new minerals and mineral names. Canadian Mineralogist, 35, 1571–1606.

Croce, A., Allegrina, M., Rinaudo, C., Gaudino, G., Yang, H., and Carbone, M. (2015) Numerous iron-rich particles lie on the surface of erionite fibers from Rome (Oregon, USA) and Karlik (Cappadocia, Turkey). Microscopy and Microanalysis, 21, 1341–1347.

Deffeyes, K.S. (1959) Erionite from Cenozoic tuffaceous sediments, central Nevada. American Mineralogist, 44, 501–509.

Dogan, M. (2012) Quantitative characterization of the mesothelioma-inducing erionite series minerals by transmission electron microscopy and energy dispersive spectroscopy. Scanning, 34, 37–42.

Dogan, A.U., and Dogan, M. (2008) Re-evaluation and re-classification of erionite series minerals. Environmental Geochemistry and Health, 30, 355–366.

Eakle, A.S. (1898) Erionite, a new zeolite. American Journal of Science, 6, 66–68.

Gude, A.J., and Sheppard, R.A. (1981) Woolly erionite from the Reese River zeolite deposit, Lander County, Nevada, and its relationship to other erionites. Clays and Clay Minerals, 29, 378–384.

Hay, R.L. (1964) Phillipsite of saline lakes and soils. American Mineralogist, 49, 1366–1387.

——— (1966) Zeolites and zeolitic reactions in sedimentary rocks. Geological Society of America Special Paper, 85, 130 pp

Henke, B.L. (1985) Scattering factors and mass absorption coefficients. In D. Vaughan, Ed., X-ray Data Booklet, chapter 2.7. Center for X-ray Optics, Lawrence Berkeley Laboratory, Berkeley, California.

Hoss, H., and Roy, R. (1960) Zeolite Studies III: On natural phillipsite, gismondite, harmatome, chabazite, and gmelinite. Beiträge zur Mineralogieund Petrographie, 7, 389–408.

Jiang, N., and Spence, J.C.H. (2012) On the dose-rate threshold of beam damage in TEM. Ultramicroscopy, 113, 78–82.

Lowers, H.A., Adams, D.T., Meeker, G.P. and Nutt, C.J. (2010) Chemical and Morphological Comparison of Erionite from Oregon, North Dakota, and Turkey. U.S. Geological Survey Open-File Report 2010-1286, Reston, Virginia.

Martin, J., Beauparlant, M., Sauvé, S., and Espérance, G. (2016) On the threshold conditions for electron beam damage of asbestos amosite fibers in the transmission electron microscope (TEM). Journal of Occupational and Environmental Hygiene, 12, 924–935.

Matassa, R., Familiari, G., Relucenti, M., Battaglione, E., Downing, C., Pacella, A., Cametti, G., and Ballirano, P. (2015) A deep look into erionite fibres: an electron microscopy investigation of their self-assembly. Scientific Reports, 5, 16757.

Mattioli, M., Giordani, M., Dogan, M., Cangiotti, M., Avella, G., Giorgi, R., Dogan, A.U., and Ottaviani, M.F. (2016) Morpho-chemical characterization and surface properties of carcinogenic zeolite fibers Journal of Hazardous Materials, 305, 140–148

Mumpton, F.A. (1979) Reconnaissance study of the association of zeolites with mesothelioma cancer occurrences in central Turkey. Society of Mining Engineers of AIME Preprint Number 79-332, presented at SME-AIME Fall Meeting, Tucson, Arizona, October 17–19, 23 pp.

Mumpton, F.A., and Ormsby, W.C. (1976) Morphology of zeolites in sedimentary rocks by scanning electron microscopy. Clays and Clay Minerals, 24, 1–23.

Nielsen, C.H., and Sigurdsson, H. (1981) Quantitative methods for electron microprobe analysis of sodium in in natural and synthetic glasses. American Mineralogist, 66, 547–552.

Passaglia, E., Artioli, G., and Gualtieri, A. (1998) Crystal chemistry of the zeolites erionite and offretite. American Mineralogist, 83, 577–589.

Purvis, K. (1991) Fibrous clay mineral collapse produced by beam damage of carbon-coated samples during scanning electron microscopy. Clay Minerals, 26, 141–145.

Rohl, A.N., Langer, A.M., Moncure, G., Selikoff, I.J. and Fischbein. A. (1982) Endemic pleural disease associated with exposure to mixed fibrous dust in Turkey. Science, 216, 518–520.

Saini-Eidukat, B., and Triplett, J.W. (2014) Erionite and offretite from the Killdeer Mountains, Dunn County, North Dakota, U.S.A. American Mineralogist, 99, 8–15.

Sheppard, R.A. (1996) Occurrences of erionite in sedimentary rocks of the western United States. U.S. Department of the Interior, U.S. Geological Survey Open-File Report 96-018, 24 pp. Denver, Colorado.

Simonato, L., Baris, R., Saracci. R., Skidmore, J., and Winkelmann, R. (1989) Relation of environmental exposure to erionite fibres to risk of respiratory cancer. International Agency for Research on Cancer (IARC) Scientific Publications, 90, 398–405.

Steel, E.B., and Small, J.A. (1985) Accuracy of transmission electron microscopy for the analysis of asbestos in ambient environments. Analytical Chemistry, 57, 209–213.

Ugurlu, O., Haus, J., Thomas, M.G., Maheshwari, S., Tsapitis, M., and Mkhoyan, K.A. (2011) Radiolysis to knock-on damage transition in zeolites under electron beam irradiation. Physics Reviews B, 83, 113408.

Van Gosen, B.S., Blitz, T.A., Plumlee, G.S., Meeker, G.P., and Pierson, M.P. (2013) Geologic occurrences of erionite in the United States: an emerging national public health concern for respiratory disease. Environmental Geochemistry and Health, 35(4), 419–430.

Zusmann, J., and Brindley, G.W. (1957) Electron diffraction studies of serpentine minerals. American Mineralogist, 42, 133–153.

MANUSCRIPT RECEIVED JANUARY 5, 2017
MANUSCRIPT ACCEPTED APRIL 28, 2017
MANUSCRIPT HANDLED BY LYNDA WILLIAMS